CONFERENCE PRE-PRINT

BOUT++ SIMULATION STUDY OF THE EFFECT OF RESONANT MAGNETIC PERTURBATION ON THE TURBULENCE TRANSPORT

S.F. MAO

School of Nuclear Science and Technology, University of Science and Technology of China Hefei, China

Email: sfmao@ustc.edu.cn

Z.M. ZHEN

School of Nuclear Science and Technology, University of Science and Technology of China Hefei, China

M.Y. YE

School of Nuclear Science and Technology, University of Science and Technology of China Hefei, China

Abstract

According to the BOUT++ simulation based on the six-field two-fluid model where the influence of resonant magnetic perturbation (RMP) response field is introduced, the turbulent particle transport is found to dominate the particle transport maintaining the edge plasma profile after edge localized mode (ELM) suppression by applying n = 4 RMP (3 kA coil current) in EAST experiment. To further explore the correlation between the turbulent particle flux with the RMP field strength, the BOUT++ simulations are performed under a series of RMP coil current. While the growth rate of the pressure perturbation increases with the RMP current, both the saturated pressure perturbation amplitude and the turbulent transport flux exhibit non-monotonic dependence, which reflects the complicated effect on non-linear mode coupling due to the RMP response field. As the turbulent particle flux peaks at ~ 1 kA RMP current, which is lower than the threshold current for ELM suppression in EAST experiment, further simulation study should be conducted based on the edge plasma profile before ELM suppression.

1. INTRODUCTION

The resonant magnetic perturbation (RMP) has been demonstrated as an effective way for controlling edge-localized modes (ELMs). Accompanied with the RMP-induced ELM suppression, the density pump-out phenomenon [1-3] has been also observed. Several mechanisms have been proposed to explain this phenomenon. One possible mechanism is the forming of magnetic islands in the pedestal region or the stochastic magnetic fields at the edge, both of which enhance radial particle transport [4, 5]. The neoclassical toroidal viscosity (NTV) effects [6] due to the break of the toroidal symmetry of the equilibrium magnetic field is also considered as a possible mechanism. Enhanced turbulent transport also contribute to the density pump-out. After the suppression of ELM using resonant magnetic perturbations (RMPs) in devices such as EAST [7] and DIII-D [8, 9], an enhancement in edge plasma fluctuations has been observed.

In our previous work [10], based on the BOUT++ simulation, it is found that the simulated flux-surface averaged radial particle flux at the position of peak pressure gradient is \sim 1.5 times when considering the influence of the RMP response field based on the EAST experimental edge plasma profiles after ELM suppression by n=4 RMP with 3 kA coil current. The simulated turbulent particle flux is close to the particle flux estimated according to the experimental plasma profiles, which implies that the turbulence transport could have a dominating contribution to the radial transport for maintaining the pedestal density profile after density pump-out.

To further explore the correlation between the turbulent particle flux with the RMP response field strength, BOUT++ simulations are performed based on the RMP response fields obtained by CLTx [11] simulations for a series of RMP coil currents.

2. SIMULATION MODEL

To simulate the edge plasma turbulence, the BOUT++ six-field two-fluid model [12] is adopted:

$$\frac{\partial \boldsymbol{\varpi}}{\partial t} = -\frac{1}{B_0} \boldsymbol{b} \times \nabla_{\perp} \boldsymbol{\Phi} \cdot \nabla \boldsymbol{\varpi} + B_0^2 \nabla_{\parallel} \left(\frac{J_{\parallel}}{B_0} \right) + 2 \boldsymbol{b} \times \boldsymbol{\kappa} \cdot \nabla P_{i}
- \frac{1}{2\Omega_{i}} \left[\frac{1}{B_0} \boldsymbol{b} \times \nabla P_{i} \cdot \nabla \left(\nabla_{\perp}^{2} \boldsymbol{\Phi} \right) - Z_{i} e B_0 \boldsymbol{b} \times \nabla n_{i} \cdot \nabla \left(\frac{\nabla_{\perp} \boldsymbol{\Phi}}{B_0} \right)^{2} \right]
+ \frac{1}{2\Omega_{i}} \left[\frac{1}{B_0} \boldsymbol{b} \times \nabla \boldsymbol{\Phi} \cdot \nabla \left(\nabla_{\perp}^{2} P_{i} \right) - \nabla_{\perp}^{2} \left(\frac{1}{B_0} \boldsymbol{b} \times \nabla \boldsymbol{\Phi} \cdot \nabla P_{i} \right) \right] + \mu_{\parallel i} \nabla_{\parallel 0}^{2} \boldsymbol{\varpi}$$
(1)

$$\frac{\partial n_{i}}{\partial t} = -\frac{1}{B_{0}} \boldsymbol{b} \times \boldsymbol{\nabla}_{\perp} \boldsymbol{\Phi} \cdot \boldsymbol{\nabla} n_{i} - \frac{2n_{i}}{B_{0}} \boldsymbol{b} \times \boldsymbol{\kappa} \cdot \boldsymbol{\nabla} \boldsymbol{\Phi} - \frac{2}{Z_{i} e B_{0}} \boldsymbol{b} \times \boldsymbol{\kappa} \cdot \boldsymbol{\nabla} P_{i} - n_{i} B_{0} \boldsymbol{\nabla}_{\parallel} \left(\frac{V_{\parallel i}}{B_{0}} \right), \tag{2}$$

$$\frac{\partial V_{\parallel i}}{\partial t} = -\frac{1}{B_0} \boldsymbol{b} \times \nabla_{\perp} \boldsymbol{\Phi} \cdot \nabla V_{\parallel i} - \frac{1}{m_i n_{i0}} \boldsymbol{b} \cdot \nabla P, \qquad (3)$$

$$\frac{\partial A_{\parallel}}{\partial t} = -\nabla_{\parallel} \phi + \frac{\eta}{\mu_0} \nabla_{\perp}^2 A_{\parallel} + \frac{1}{e n_{e0} B_0} \nabla_{\parallel} P_{e} + \frac{0.71 k_{\rm B}}{e B_0} \cdot \nabla_{\parallel} T_{e} - \frac{\eta_{\rm H}}{\mu_0} \nabla_{\perp}^4 A_{\parallel}, \tag{4}$$

$$\frac{\partial T_{i}}{\partial t} = -\frac{1}{B_{0}} \boldsymbol{b} \times \nabla_{\perp} \Phi \cdot \nabla T_{i}$$

$$-\frac{2}{3} T_{i} \left[\left(\frac{2}{B_{0}} \boldsymbol{b} \times \boldsymbol{\kappa} \right) \cdot \left(\nabla \Phi + \frac{1}{Z_{i} e n_{i0}} \nabla P_{i} + \frac{5}{2} \frac{k_{B}}{Z_{i} e} \nabla T_{i} \right) + B_{0} \nabla_{\parallel} \left(\frac{V_{\parallel i}}{B_{0}} \right) \right],$$

$$+ \frac{2}{3 n_{i0} k_{B}} \nabla_{\parallel 0} \left(\kappa_{\parallel i} \nabla_{\parallel 0} T_{i} \right) + \frac{2}{3 n_{i0} k_{B}} \nabla_{\perp} \cdot \left(\kappa_{\perp i} \nabla_{\perp} T_{i} \right) + \frac{2 m_{e}}{m_{i}} \frac{Z_{i}}{T_{e}} \left(T_{e} - T_{i} \right)$$
(5)

$$\frac{\partial T_{e}}{\partial t} = -\frac{1}{B_{0}} \boldsymbol{b} \times \nabla_{\perp} \Phi \cdot \nabla T_{e}$$

$$-\frac{2}{3} T_{e} \left[\left(\frac{2}{B_{0}} \boldsymbol{b} \times \boldsymbol{\kappa} \right) \cdot \left(\nabla \Phi - \frac{1}{e n_{e0}} \nabla P_{e} - \frac{5}{2} \frac{k_{B}}{e} \nabla T_{e} \right) + B_{0} \nabla_{\parallel} \left(\frac{V_{\parallel e}}{B_{0}} \right) \right]$$

$$+ 0.71 \frac{2T_{e}}{3e n_{e0}} B_{0} \nabla_{\parallel} \left(\frac{J_{\parallel}}{B_{0}} \right) + \frac{2}{3n_{e0} k_{B}} \nabla_{\parallel 0} \left(\kappa_{\parallel e} \nabla_{\parallel 0} T_{e} \right) + \frac{2}{3n_{e0} k_{B}} \nabla_{\perp} \cdot \left(\kappa_{\perp e} \nabla_{\perp} T_{e} \right)$$

$$-\frac{2m_{e}}{m_{i}} \frac{1}{\tau_{e}} \left(T_{e} - T_{i} \right) + \frac{2}{3n_{e0} k_{B}} \eta_{\parallel} J_{\parallel}^{2}$$
(6)

where

$$\boldsymbol{\varpi} = n_{i0} \frac{m_{i}}{B_{0}} (\nabla_{\perp}^{2} \phi + \frac{1}{n_{i0}} \nabla_{\perp} \phi \cdot \nabla_{\perp} \phi + \frac{1}{n_{i0} Z_{i} e} \nabla_{\perp}^{2} p_{i1}), \qquad (7)$$

$$J_{\parallel} = J_{\parallel 0} - \frac{1}{\mu_0} B_0 \nabla_{\perp}^2 \psi , \qquad (8)$$

$$V_{\parallel e} = V_{\parallel i} + \frac{1}{\mu_0 Z_i e n_i} \nabla_{\perp}^2 A_{\parallel}. \tag{9}$$

All the variables F can be written as $F = F_0 + F_1$, where F_0 means the equilibrium part and F_1 is the perturbed part. A_{\parallel} is the parallel vector potential, $\mathbf{b} = \mathbf{b}_0 + \mathbf{b}_1 = \mathbf{b}_0 + \nabla A_{\parallel} \times \mathbf{b}_0 / B$ is the unit vector of the total magnetic field, and $K = \mathbf{b}_0 \cdot \nabla \mathbf{b}_0$. The operators are defined as $\nabla_{\parallel 0} = \mathbf{b}_0 \cdot \nabla$, $\nabla_{\parallel} = \nabla_{\parallel 0} + \mathbf{b}_1 \cdot \nabla$ and $\nabla_{\perp} = \nabla - \mathbf{b} \nabla_{\parallel}$.

The perturbation field induced by RMP B_{RMP} is introduced in the simulation according to Dong et al.'s work [13]. Compared with the total field

$$\boldsymbol{B}_{0}' = \boldsymbol{B}_{0} + \boldsymbol{B}_{\text{RMP}}, \tag{10}$$

the strength of B_{RMP} is usually about 4 orders of magnitude lower. Therefore,

$$B_0' = |B_0'| = |B_0 + B_{RMP}| \approx |B_0| = B_0 \tag{11}$$

and the unit vector of B_0'

$$\boldsymbol{b}_{0}' = \frac{\boldsymbol{B}_{0} + \boldsymbol{B}_{\text{RMP}}}{B_{0}'} \approx \frac{\boldsymbol{B}_{0}}{B_{0}} + \frac{\boldsymbol{B}_{\text{RMP}}}{B_{0}} = \boldsymbol{b}_{0} + \frac{\boldsymbol{B}_{\text{RMP}}}{B_{0}}.$$
(12)

To introduce the influence of RMP field, b_0 in the six-field two-fluid model is substituted by b'_0 , and the parallel differential operator is also modified:

$$\nabla_{\parallel 0} F = \boldsymbol{b}_0 \cdot \nabla F + \frac{\boldsymbol{B}_{\text{RMP}}}{B_0} \cdot \nabla F . \tag{13}$$

 $\boldsymbol{B}_{\text{RMP}}$ is calculated by CLTx, which is an extended version of the cylindrical coordinate three-dimensional magnetohydrodynamic code CLT. In CLTx, the scrape-off layer can be self-consistently simulated, and a RMP module is developed for calculating the plasma response field to RMP.

By applying n = 4 RMP (coil current 3 kA, with a 180° phase difference between the upper and lower coil sets) in EAST discharge #94048 [14], ELM suppression is achieved. The equilibrium at 5.9 s and the corresponding edge plasma profiles are used for the simulation study. As shown in Fig. 1, the RMP coil current is scanned from 2 kA to 4 kA. Fig. 1(a) shows the radial distribution of m/n = 20/4 resonant component for the vacuum field under different RMP coil current, while Fig. 1(b) shows the results for the response field. It clearly reflects the screening effect on the RMP field penetration. For all the resonant components, the amplitudes increase linearly with the RMP coil current, as shown for the 20/4 component in Fig. 2.

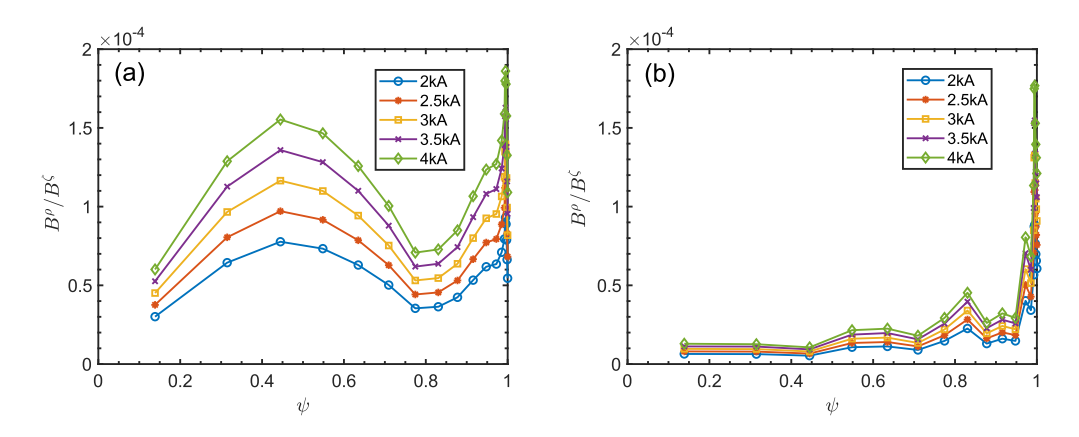


Figure 1. Radial distribution of 20/4 component under different RMP coil currents for (a) vacuum field and (b) response fields.

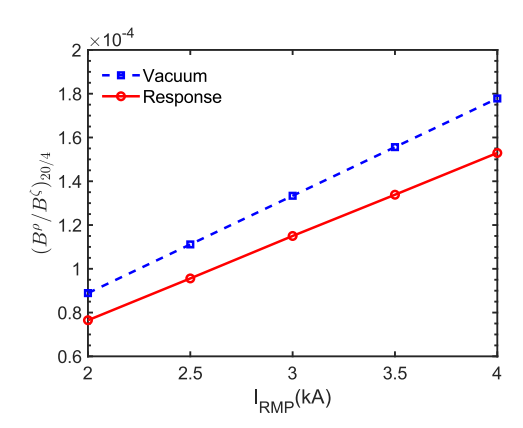
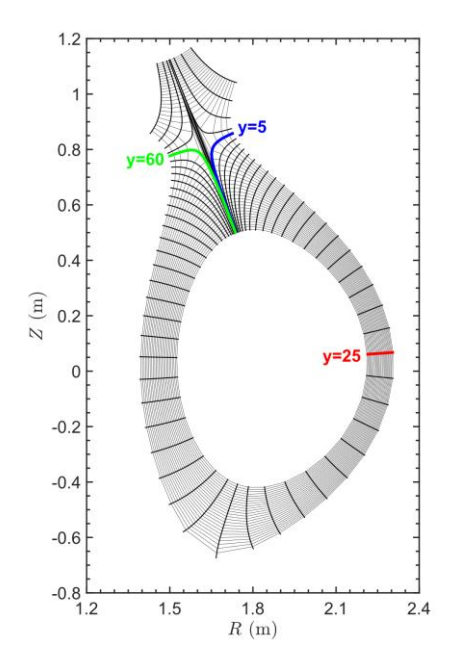


Figure 2. Dependence of the amplitude of 20/4 component on the RMP coil current.



 $Figure\ 3.\ BOUT++\ simulation\ grid.$

The BOUT++ simulation region covers the pedestal and the scrape-off layer (SOL) for $\psi = 0.7 \sim 1.05$, where ψ is the normalized poloidal magnetic flux. Fig. 3 shows the grid for BOUT++ simulation. The grid sizes are $256 \times 64 \times 64$ in the (x, y, z) directions. The simulation is performed within 1/4 tours for saving computational resource.

3. RESULTS AND DISCUSSION

The time evolutions of the toroidal root-mean-square (RMS) of pressure perturbations at the position of peak pressure gradient in the outer mid-plane are shown in Fig. 4. It should be noted that, the response fields of 0.5 kA and 1 kA RMP coil currents are obtained by linear interpolation. It can be seen that, the growth rate of the pressure perturbation increases with the RMP coil current. In the present BOUT++ simulation model, the response field is introduced directly on the equilibrium magnetic field, and thus acts as an additional driving source.

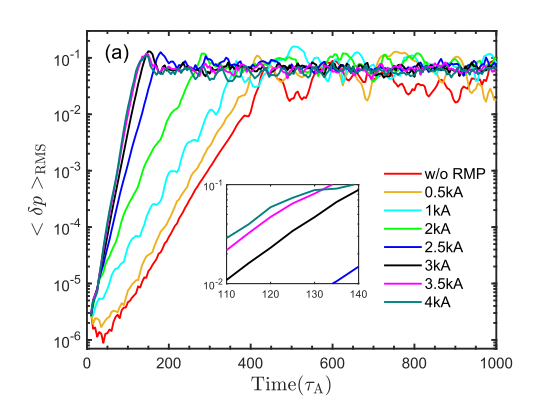


Figure 4. Time evolution of the RMS pressure perturbations under different RMP coil currents at the peak pressure gradient at the outer mid-plane.

During the nonlinear saturation phase, the RMS pressure perturbation at $\psi = 097$ in the outer mid-plane is average over $600\sim1000~\tau_A$. The dependence of time averaged amplitude of the pressure perturbation on the RMP coil current is shown in Fig. 5. It can be clearly seen the non-monotonic dependence on the RMP coil current, which reflects the complicated effect on non-linear mode coupling due to the RMP response field.

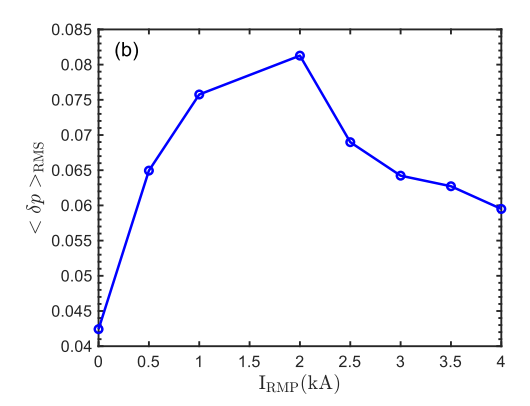
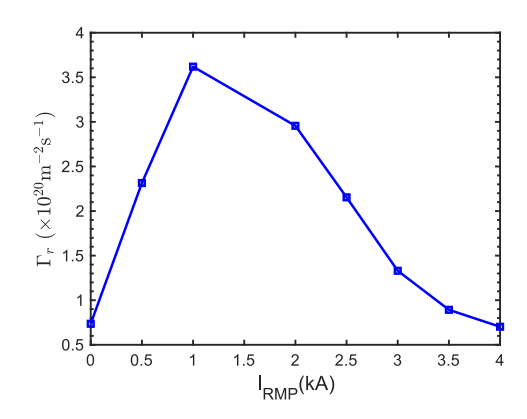


Figure 5. Dependence of the time averaged (over 600~1000 \tau A during the nonlinear saturation phase) RMS pressure perturbation on the RMP coil current.



 $Figure\ 6.\ Dependence\ of\ the\ time\ averaged\ radial\ particle\ flux\ on\ the\ RMP\ coil\ current.$

The time averaged (over $600\sim1000~\tau_A$) radial particle flux at $\psi=097$ in the outer mid-plane is further shown in Fig. 6 for different RMP coil currents. The non-monotonic dependence also appears. The radial particle flux peak

is at ~ 1 kA RMP coil current, while the peak of the pressure perturbation peaks at ~ 2 kA. As mentioned in our previous work, the RMP response field could lead to a inward magnetic flutter flux accompanied with strong outward electric drift flux. Moreover, it is interesting that the threshold of RMP coil current for ELM suppression is ~ 3 kA, which is much larger than that for the radial particle flux peak. It is easy to understand that a higher RMP coil current is required to have a sufficient penetration depth of the RMP field before ELM suppression. From the point of density profile evolution, for the same RMP coil current, the radial turbulent flux may peak at 3 kA before density pump-out, and then decrease to a certain level to maintain the density profile after density pump-out. To examine the hypothesis, it is required further simulation study based on the edge plasma profile before ELM suppression

4. CONCLUSION

The dependence of the turbulent particle flux on the RMP coil current is studied by BOUT++ simulation with the influence of RMP response field in the present work. It is found that, although the growth rate of the pressure perturbation increase with the RMP coil current, the saturated pressure perturbation and the turbulent transport flux show the non-monotonic dependence on the RMP coil current. The radial particle flux peaks about 1 kA RMP coil current, which is much lower than the 3 kA threshold for ELM suppression. Further simulation study is required for understanding the density profile evolution regarding the density pump-out and maintain of the density profile after ELM suppression.

ACKNOWLEDGEMENTS

This work is supported by the National MCF Energy R&D Program of China (Grant No. 2024YFE03010003, 2019YFE03080500, 2019YFE03030004). Numerical simulations are carried out using the CFETR Integration Design Platform (CIDP) with the support of the Supercomputing Center of University of Science and Technology of China.

REFERENCES

- [1] Wang S.X. et al., Investigation of RMP induced density pump-out on EAST, Nucl. Fusion 58 (2018) 112013.
- [2] Hu Q.M. et al., The role of edge resonant magnetic perturbations in edge-localized-mode suppression and density pumpout in low-collisionality DIII-D plasmas, Nucl. Fusion **60** (2020) 076001.
- [3] Leuthold N. et al., Turbulence characterization during the suppression of edge-localized modes by magnetic perturbations on ASDEX Upgrade, Nucl. Fusion **63** (2023) 046014.
- [4] Sun Y. et al., Edge localized mode control using n = 1 resonant magnetic perturbation in the EAST tokamak, Nucl. Fusion 57 (2016) 036007.
- [5] Chang Y.Y. et al., Tungsten transport due to the neoclassical toroidal viscosity induced by resonant magnetic perturbation in the EAST tokamak, Phys. Plasmas **30** (2023) 122301.
- [6] Zhang N. et al., Toroidal modeling of plasma flow damping and density pump-out by RMP during ELM mitigation in HL-2A, Nucl. Fusion **63** (2023) 086019.
- [7] Liu S.C. et al., Edge turbulence transport during ELM suppression with n = 4 resonant magnetic perturbation on EAST, Nucl. Fusion **63** (2023) 042003.
- [8] Wilcox R.S. et al., Evidence of Toroidally Localized Turbulence with Applied 3D Fields in the DIII-D Tokamak, Phys. Rev. Lett. **117** (2016) 135001.
- [9] Mckee G.R., Increase of turbulence and transport with resonant magnetic perturbations in ELM-suppressed plasmas on DIII-D, Nucl. Fusion **53** (2013) 113011.
- [10] Zhen Z.M. et al., BOUT++ simulation study of the turbulence transport during n = 4 resonant magnetic perturbation induced edge localized mode suppression phase in EAST, Chin. Phys. B (accepted). DOI: 10.1088/1674-1056/ae04d8.
- [11] Wang S. et al., Influence of toroidal rotation on resistive tearing modes in tokamaks, Phys. Plasmas 22 (2015) 122504.
- [12] Xia T.Y. et al., Six-field two-fluid simulations of peeling-ballooning modes using BOUT++, Nucl. Fusion **53** (2013) 073009.
- [13] Dong L.K. et al., The effect of the plasma response on peeling–ballooning modes during edge localized modes mitigated by resonant magnetic perturbations, Nucl. Fusion **63** (2023) 086023.
- [14] Sun Y. et al., First demonstration of full ELM suppression in low input torque plasmas to support ITER research plan using n=4 RMP in EAST, Nucl. Fusion **61** (2021) 106037.